Thermodynamic Modeling of Elemental Distributions of Trace Elements in Non-ferrous Iron Residue Hydrogen Reduction

IIDA PANKKA [1,3] JUSTIN SALMINEN,[2] PEKKA TASKINEN [1] and DANIEL LINDBERG [1]

1.—Department of Chemical and Metallurgical Engineering, School of Chemical Engineering, Aalto University, Espoo, Finland. 2.—Boliden Kokkola, Kokkola, Finland. 3.—e-mail: iida.pankka@aalto.fi

Every year millions of tons of iron residue are generated as a by-product of zinc production. Stabilized landfilled iron residue contains recoverable metals that could be valorized with further processing. Pyrometallurgical processing allows the recovery of valuable metals while simultaneously producing a clean slag that can then be further utilized. A thermodynamic model was developed with FactSage version 8.0. The focus was on minor element behavior and distribution of elements between phases. Calculations were performed at 1200–1400°C and pressure of 1 atm with both pure H_2 and H_2-Ar mixtures used as a reductant. Also, the concentrations of Pb and Zn in the input were varied. The results showed that a liquid alloy phase forms consisting mostly of either Cu, As and Pb or Fe, As and Cu. It was noted that a higher Ar total gas amount in reduction decreased the mass fraction of the liquid alloy and increased the evaporation of elements into fume dust. S, Bi, Pb, Ge and Zn were observed to evaporate fully, while As, In, Sb and Ag evaporated only partially. The results need to be verified experimentally.

INTRODUCTION

Zinc is mainly used for galvanizing iron and steel, die-casting as well as an alloying metal to make bronze and brass. In 2021 the world zinc mine production was 12.8 Mt and refined zinc production was 13.8 Mt.[1] Iron is an unwanted component in zinc sulfide concentrates and calcines from secondary sources.

The roasting-leaching-electrowinning is the dominant route in zinc production.[2] In recent decades, atmospheric direct concentrate leaching has gained attention[3] where most sulfur remains in the leaching residue in elemental form with some unleached sulfides, like PbS and FeS. The desired metals can be leached from the concentrates along with some iron, but iron represents the largest impurity in zinc sulfate solutions and must be removed before electrowinning.[4] A common way to remove iron in hydrometallurgical processing is through jarosite precipitation.[5] The general formula for jarosite is $M[Fe_3(SO_4)_2(OH)_6]$, where M represents H_3O^+, Na^+, K^+, NH^{4+}, Ag^+, Li^+ or Pb^{2+}.[6] In addition, some elements, e.g., Zn, Cd, Ni and Co may replace Fe in the crystal lattice of jarosite.[6–8]
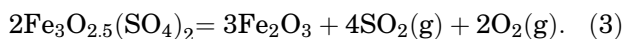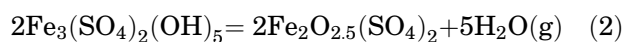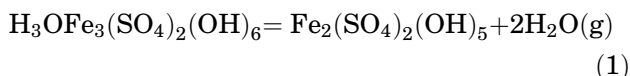
The aim towards circular economy has increased the interest in processing residues into usable forms. Of course, improved yields and resource efficiency are major incentives as well. Instead of simply landfilling the combined residue, a more sustainable solution would be to recover valuable metals from the residue, while simultaneously producing an inert slag that could be utilized in, for example, road building or construction material applications.[9] Recovery of minor elements such as indium and silver can improve economics of a recycling process.[10] Many of these trace metals are also defined as critical in the EU, making their recovery even more important. For example, in the case of indium where the recovery from ores is only around 35%, this means that 65% of mined indium ends up in landfills of the mining site and smelters.[10]

Three broad approaches have been proposed to treat zinc residue: stabilization, hydrometallurgical processing and pyrometallurgical processing.[11,12] Stabilization ends up with a product that can be re-classified as stable waste, but it doesn't involve metal recovery. It can also be challenging to find alternative uses for stabilized products. Solidification/stabilization (s/s) is a waste treatment/management technique, widely used for immobilization/remediation of hazardous wastes because of its ability to inhibit the transport of pollutant elements into the surrounding environment as well as its ability to improve the physical characteristics, thus reducing the transport and leaching of hazardous metals.[13] Portland cement is the most common medium used in the s/s process.[14] Waste marble slurry[15] and fly ash[13] are examples of substances that can be used to immobilize the hazardous substances in jarosite.

Hydrometallurgical processes often concentrate primarily on recovering the contained metals instead of producing an inert material suitable for safe disposal.[11] There are many different lixiviants that can be used to leach valuable metals from jarosite. One example is using aqueous NH_4Cl for leaching Zn, Pb, Cu, Cd and Ag;[7] another is using of thiourea for extracting Au and Ag.[16] The Jarogain process includes leaching in a reducing environment and separating the metals to hydroxides and sulfides, the main products of the process being a lead concentrate including silver and gold, a mixed gallium, indium and germanium concentrate, a zinc concentrate, sulfuric acid as well as an iron concentrate.[17]

Pyrometallurgical processing produces a stable slag and allows for the recovery of most valuable metals.[9] The goal of a pyrometallurgical process is to produce a clean slag, while concentrating the valuable metals in other phases, such as the flue dust and metal alloy or sulfide matte.[18,19] Ausmelt Top Submerged Lance (TSL) and Waelz Kiln are examples of pyrometallurgical technologies that are used for the thermal treatment of zinc residues.[20] Also, plasma-submerged smelting[21] has recently gained industrial applications.

The purpose of this article is to model the equilibria and element deportments of a thermal treatment of an iron residue originating from iron residues of zinc production. The study focuses on reduction of already pretreated and desulfurized combined residue with variable concentrations of Zn and Pb. In the pre-treatment, essentially total desulfurization is needed for the subsequent reduction steps. For hydronium and ammonium jarosites, the desulfurization proceeds in several steps at 250–650°C[22] and can be written as

$$H_3OFe_3(SO_4)_2(OH)_6 = Fe_2(SO_4)_2(OH)_5 + 2H_2O(g) \quad (1)$$

$$2Fe_3(SO_4)_2(OH)_5 = 2Fe_2O_{2.5}(SO_4)_2 + 5H_2O(g) \quad (2)$$

$$2Fe_3O_{2.5}(SO_4)_2 = 3Fe_2O_3 + 4SO_2(g) + 2O_2(g). \quad (3)$$

The elemental sulfur and sulfides in the mixed residue will be combusted in the desulfurization step generating CO_2-free energy for smelting. The aim was to provide information on how to clean impure iron residue effectively, allowing the valuable metals to be recovered while producing an environmentally stable slag. This work improves understanding of the means by which non-ferrous residues like iron rich sludges including residues from the zinc industry can be treated to valorize valuable metals and obtain acceptable slag for the use of the construction industry, for example. The thermodynamic model on reduction of pretreated and desulfurized mixed residue was built with FactSage, version 8.0, and its databases.

METHODS

Thermodynamic databases, which are included in thermodynamic software packages, are developed based on the CALculation of PHAse Diagrams (CALPHAD) methodology.[23] The CALPHAD method is based on a stepwise approach where the unaries and binaries are modeled first, and all higher order systems are based on those assessments. The calculations were made using minimization of the Gibbs energy of the system.[24] The calculations require that thermodynamic data exist for all thermodynamic phases considered. The data for multicomponent solution phases are based on the thermodynamic data of end members, mixing rules of the solution components and the interaction parameters of the solution model.[25] The Gibbs energy functions recreate the thermodynamic properties of the phases and utilize them in predictions of unknown phase equilibria.[23] By minimizing the Gibbs energy of the system and considering the Gibbs energies of all the phases, the true chemical equilibrium can be calculated.[25] The Gibbs energy of a phase, G, can is expressed with following equation:

$$G = \sum_i n_i \mu_i \quad (4)$$

where n_i is the amount of component i and μ_i is the chemical potential (molar Gibbs energy) of component i. Equation 5 can is used to calculate the Gibbs energy of a heterogeneous system of several phases (f).

$$G = \sum_\phi N^\phi G_m^\phi \quad (5)$$

where N^φ is the amount of the phase f and G^φ_m is the Gibbs energy of the phase. The relation of Gibbs

energy to enthalpy (H), entropy (S) and heat capacity (C_p) can be expressed (above the reference temperature) with following formula:

$$G = \Delta H_{298} + \int_{298}^{T} C_p(T)dT - T\left(S_{298} + \int_{298}^{T} \frac{C_p(T)}{T}dT\right) \tag{6}$$

The Modified Quasichemical Model (MQM), which was first introduced by Pelton and Blander,[26] has been used to model thermodynamic properties of the liquid oxide phase (liquid slag). FactSage uses MQM for complex non-ideal solutions such as molten oxide, molten sulfide, molten salt and liquid metallic solutions.[23] The latest public databases for pure substances (FactPS), oxides/slags (FTOxid) and solid and liquid alloys (FSCopp) were used. The gas was treated as an ideal gas. The data for liquid slag were the latest version in the FToxid database (designated as SLAGA in the software); in addition, several dilute components that are not part of the standard data were added as dilute components based on Pelton et al.[27]

The Equilib module was applied for the calculations. It is the Gibbs energy calculation engine of the FactSage, using the Gibbs energy minimization algorithm and thermochemical functions of ChemSage.[28] Equilib executes equilibrium calculations for multicomponent and multiphase systems with the possibility to set the quantity, temperature or pressure as a variable and with suitable constraints.

The calculations were performed at 1200–1400°C in total pressure of 1 atm with the focus on minor element behavior and distributions between the different phases. Pure H_2 as well as mixture of Ar and H_2 with different ratios were used as reductants. The different Ar and H_2 mixtures were: 50 vol.% H_2 50 vol.% Ar, 25 vol.% H_2 75 vol.% Ar and 10 vol.% H_2 90 vol.% Ar.

The calculations were performed as open systems. Open system calculations are used to simulate a process where the reactants are continuously fed into the system and selected phases removed after each calculation step.[28] Figure 1 shows a diagram depicting the open system calculations. During each step, a fixed amount of the reductant was added to the slag and after equilibration the off gas removed. The product was used as the starting material for the next step. The amount of reductant added as well as the number of steps used varied between the calculations.

The slag and liquid alloy phases were set to have the possibility of including certain elements. The liquid alloy contained Ag, Al, As, Au, Bi, C, Ca, Co, Cr, Cu, Fe, Ge, H, In, Mg, Mn, Ni, O, Pb, S, Sb, Si, Sn and Zn as components. The slag contained oxides and sulfides of Al, $As^{(3+)}$, Ca, $Co^{(2+,3+)}$, $Cr^{(2+,3+)}$, $Cu^{(+)}$, $Fe^{(2+,3+)}$, Ge, K, Mg, Mn, Na, Ni, Pb, Zn, Si and $Sn^{(2+)}$ and also $Ag^{(+)}$, $Au^{(+)}$, $Bi^{(3+)}$, $Cd^{(2+)}$, $In^{(3+)}$
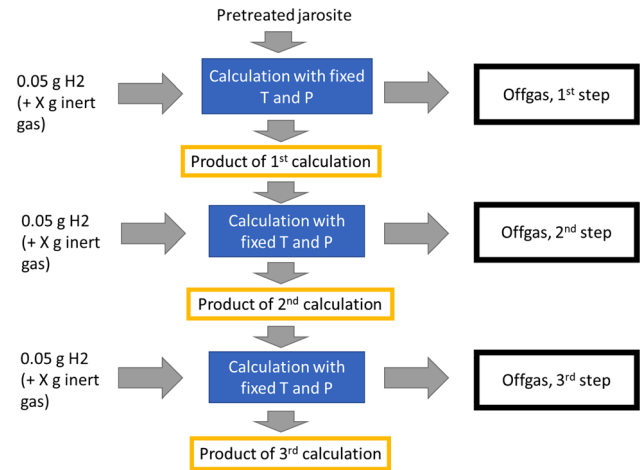

Fig. 1. Open calculations: the principle.

Table I. Pretreated jarosite composition used in the reduction step calculations

Element	Quantity (g)
Al	0.77
As	0.6[a]
Ca	7.2
Cu	0.4[a]
Fe	32.5
K	0.25
Mg	2.3
Mn	0.042
Na	1.8
O	32.25–33.05[b]
Pb	0.1–1[a]
S	0.46
Sb	0.12
Si	9.8
Sn	0.1[a]
Zn	1–4[a]

[a]An estimate.[b]Amount of oxygen was calculated from metal oxides.

and $Sb^{(3+)}$ as dilute components only. Hg and Se were not included in the slag because of the low solubility.[29]

Experimental iron residue post pretreatment was used as the input for the calculations. First, the sample was dried at 80°C in a Memmert KG oven for 22 h. Then, the pretreatment was performed in a tube furnace (Lenton LTF 16/–/450) at 700°C with an airflow of 65 mL/min for 60 min. The final desulfurization step was carried out for 60 min at 1200°C using 65 mL/min oxygen flow.[30]

Table I shows composition of pretreated jarosite used as input for the reduction calculations as well as the estimated input amounts. The oxygen amounts in Table I were calculated from the metal oxides present. All inputs for different Pb–Zn

combinations were normalized to a total of 100 g. A group of trace elements (Au, Ag, Bi, Co, Cr, Ge, In, Ni and Sn) was estimated separately for the calculations.

RESULTS AND DISCUSSION

This chapter contains simulations with the focus on minor element behavior and distributions between the different phases. The pretreated and oxidized iron residue will be referred to as the intermediate slag. All calculations were performed at 1200–1400°C in the total pressure of 1 atm, but with differing reductants and intermediate slag compositions. Calculations were performed with three different lead and zinc concentrations. Pure H_2 as well as a mixture of H_2-Ar was used as reductant. Both the slag and liquid alloy/matte phases contained numerous elements, but only certain elements of interest were highlighted in this study. The elements of interest in the slag were Bi, Pb, Au, Sb, Sn, In, Ag, As, Ge, Zn, Cu, Ni, Co, Mn and Cr. Elements of interest in the liquid alloy/matte phase were Bi, Pb, Au, Sb, Sn, In, Ag, As, Ge, Zn, Cu, Ni, Co, Fe, Mn and Cr.

Table II shows the formed phases as a function of the reductant additions. In all the cases a liquid slag, solid spinel and liquid alloy phases were formed. The spinel phase, which is a solid zinc and iron oxide rich phase $(Fe,Zn)(Fe)_2O_4$, only formed in the beginning of the calculations and disappeared after further H_2 additions. The iron solid solution phase consisted mostly of iron with some minor elements mixed in.

Figure 2 shows phase fractions for the 4% Zn 1% Pb case. The slag constitutes between 60% and 95% of the total mass. The slag phase was by far the largest phase by mass in all the cases. The liquid alloy phases, solid solution iron and gas phase are also present but only as minor phases.

Figure 2 also shows the thermodynamic reduction efficiency of hydrogen (defined as $p(H_2O)/p(H_2)$ in the off-gas) as a function of hydrogen additions in this system. The efficiency of hydrogen is around 100% until 5 kg H_2/1000 kg intermediate slag, from where it begins to rapidly decrease. At around 10 kg H_2/1000 kg intermediate slag the efficiency levels out at about 40%. No major differences in the reduction efficiency were observed between the different cases using hydrogen as the reductant.

Figure 3 shows the slag composition with the elements of interest for the 4% Zn 1% Pb. Zn is the most common element, Pb is the second, closely followed by As and Cu. These elements do not remain in the slag during the entire reduction process. Zn, Pb and mostly As evaporate gradually from the slag. Some copper remains in the slag, while most is divided between the liquid alloy and the Fe(s) solid solution.

Table II. Phases formed in the simulations of the reduction step

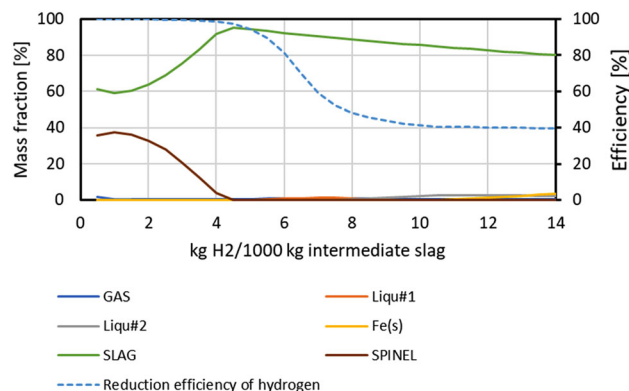| Phase names	Phase type
GAS	Gas
Liqu#1	Liquid alloy
Liqu#2	Liquid alloy (miscibility gap)
Fe (s)	Iron solid solution (with some minor elements, e.g. Cu and As)
SLAG	Molten oxide
SPINEL	Spinel

Fig. 2. Phase fractions of 4% Zn 1% Pb case with the reduction efficiency of hydrogen, showing the major phases.

Figure 4 shows the compositions of both the liquid alloy phases (miscibility gap) in the 4% Zn 1% Pb case with the dotted line indicating where each phase is present. The two liquid alloy phases are immiscible. An Au spike appeared when the amount of liquid alloy phase was very small, and thus the total mass of gold in the alloy is very small even if it makes up > 70 wt.% of the total composition of the liquid phase. Cu, As and Pb are the main elements deporting in Liquid 1. Fe forms around 80 wt.% of Liquid 2, making it clearly the most abundant element. After iron, Cu and As are the most common elements in Liquid 2.

Figure 5 shows the cumulative evaporation of elements as the function of oxygen partial pressure in the case with 4% Zn and 1% Pb. S, Bi, Pb, Ge and Zn evaporated fully, while As, In, Sb and Ag evaporated between 30% and 70%. The evaporation of Al, Ca, Co, Cr, Cu, Fe, Mg, Mn, Na and Ni is not shown in Fig. 5 because of the small percentage evaporated. Elements, such as Hg, Se and Cd, already evaporated during early stages of the thermal treatment. Therefore, they have not been included in the calculation. It can also be noted that Au and Bi seem to evaporate at relatively high oxygen partial pressure, whereas elements such as Zn and In evaporate only once the oxygen partial pressure reaches around 10^{-11} atm. However, it
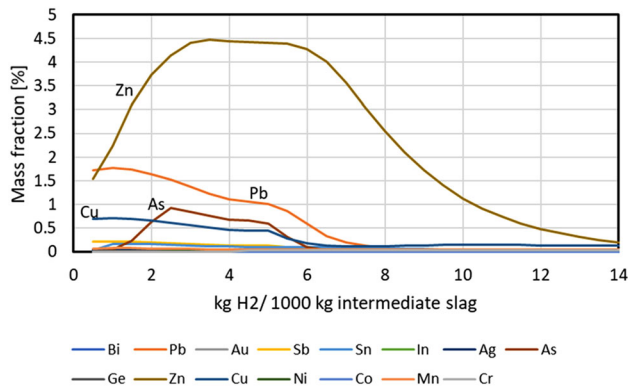
Fig. 3. Composition of slag as a function of hydrogen additions showing the elements of interest.
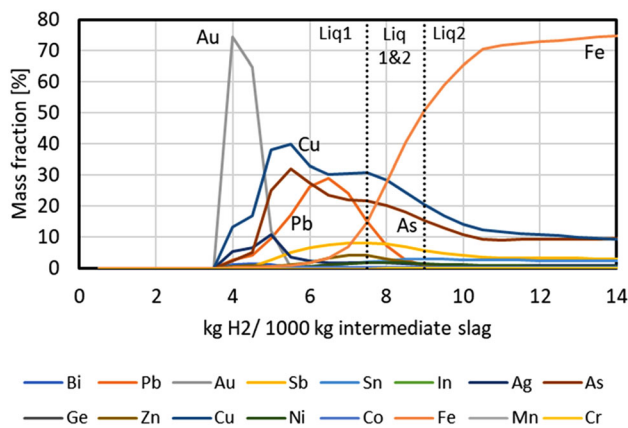

Fig. 4. Liquid alloy 1 and 2 phase composition as a function of hydrogen additions showing the elements of interest.
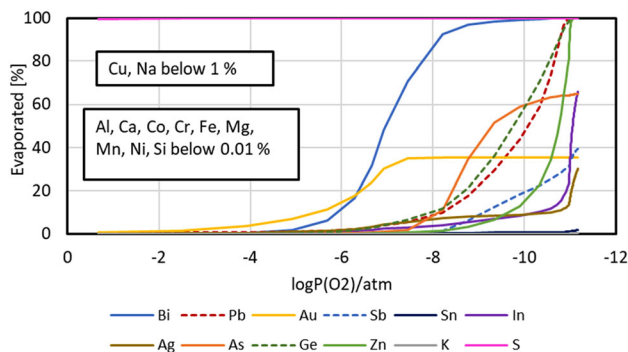

Fig. 5. Cumulative evaporation of elements as a function of oxygen partial pressure of reduction system at 1300°C collected from series of open calculation steps.

Fig. 6. Phases of the of 50 vol.% H_2 case with maximum mass fraction of 2% as ordinate axis indicating the effect of gas volumetric rate on the phase fractions (Color figure online).

should be noted that the evaporation of Bi observed in Fig. 3 is considerably higher than for example in that obtained in a computational thermodynamics model of Swinbourne and Kho.[30]

Calculations were done with three H_2-Ar mixtures: 50 vol.% H_2-50 vol.% Ar, 25 vol.% H_2-75 vol.% Ar and 10 vol.% H2-90 vol.% Ar; 4% Zn and 1% Pb were used as the input for all cases. The calculations were stopped at 15 kg H_2/1000 kg intermediate slag
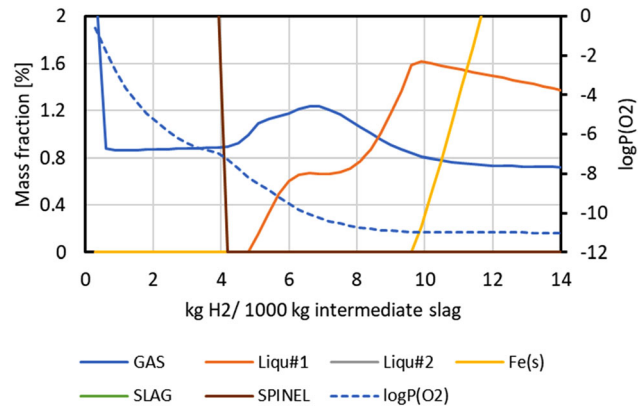
to avoid large quantities of metallic iron from forming. Figures 6, 7 and 8 show the phase distributions of the cases with 10–50 vol.% H_2, the mass fraction being up to 2 wt.%, so that the development of liquid alloy phases can be seen more clearly. The prevailing oxygen partial pressure is shown as a dotted blue line in the graphs.

It can be observed that the liquid phase fraction becomes smaller when the hydrogen is diluted and Ar fraction in the reduction gas mixture rises. It can also be observed that unlike in the base case, only one liquid phase forms in the cases with 50 and 25 vol.% H_2. Even in the case with 10 vol.% H_2, the two liquid phases do not form like in the base case, were Liquid 1 disappears shortly after Liquid 2 phase has been formed. Instead, Liquid 2 phase is a small, with a mass fraction of $\leq 0.1\%$, present between 8 kg H_2 and 1000 kg intermediate slag and 12 kg H_2/1000 kg intermediate slag.

Figures 9 and 10 show the distributions of Ag and Sb between the different phases. In cases were the H_2 was lower (larger dilution in the feed), a larger portion of Ag and Sb evaporated into the off-gas. For both Ag and Sb, this means that as a higher mass fraction evaporates a lower mass fraction deport to the liquid alloy phase. In the 50% H_2 case, only 40% of Ag and 50% Sb has evaporated, considerably less than in the 10% H_2 case where 100% of Ag and 85% Sb evaporated. For the distributions of Pb, In, Ge, Cu, As and Zn between the different phases, please refer to online supplementary material. A similar trend in the increase of the mass fraction of the gas phase can be observed with other elements, such as As and In; see supplementary Figures S-1 and S-2. Cu is an exception to this though, as hardly any of it goes into the gas phase; see supplementary Figure S-3. Another observation is that when the percentage of H_2 in the input is lower, less H_2 is needed for the same amount to evaporate—a consequence of the assumption made on the condensed-gas equilibria of the species in this study.
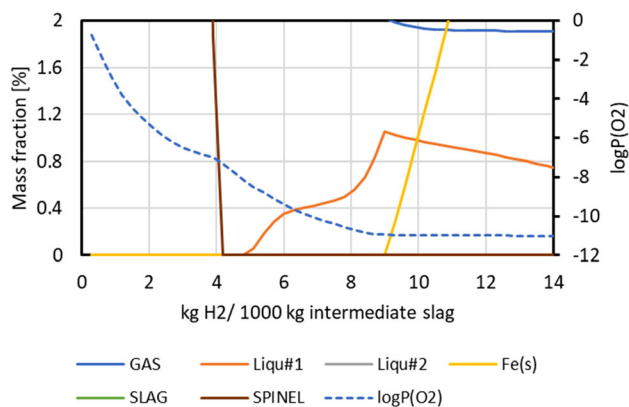
Fig. 7. Phase fractions of 25 vol.% H_2 case with maximum mass fraction of 2%, showing the formation of one liquid alloy only (Color figure online).
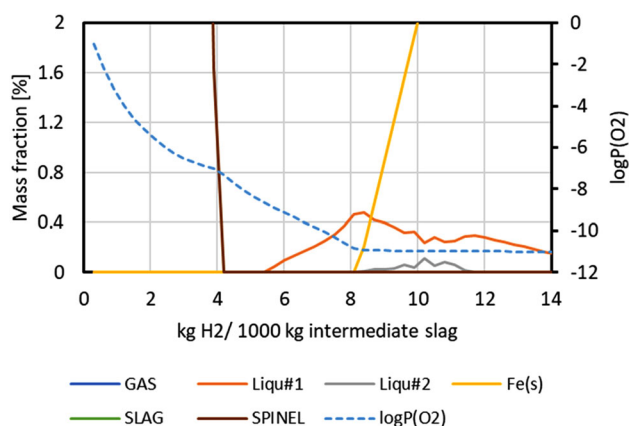

Fig. 8. Phase fractions of 10 vol.% H_2 case with maximum mass fraction of 2% showing the presence of the second liquid alloy phase in very reducing conditions after stabilizing elemental iron in the system (Color figure online).
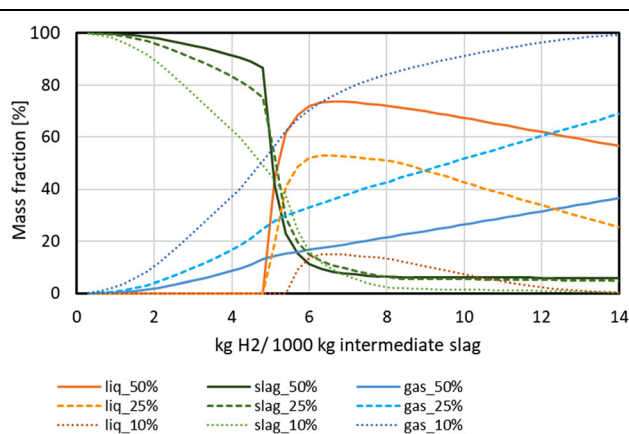

Fig. 9. Distributions of silver between different phases in the 50, 25 and 10 vol.% H_2 dilution cases of the reduction gas.
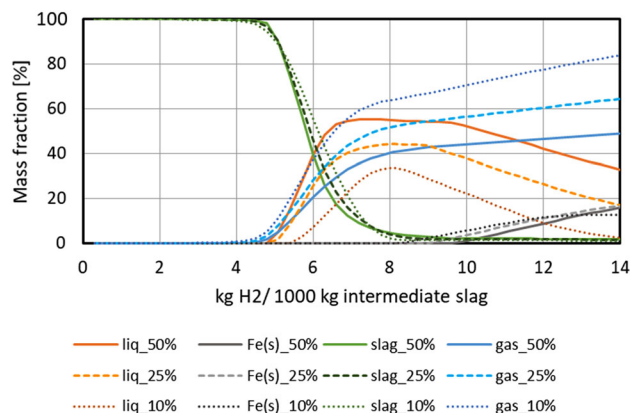
Fig. 10. Distribution of antimony between the different phases in the 50, 25 and 10 vol.% H_2 cases where the increasing total gas volume flushes antimony from the bath.

that the Sb that does not evaporate can mostly be found in the liquid alloy and solid iron solution phase. Out of the other elements that evaporate partially, As deports strongly into the liquid alloy phase while In mostly divides between the slag and liquid alloy. Pb, Ge and Zn evaporated fully; see supplementary Figures S-4, S-5 and S-6.

The formation of solid solution iron phase can be considered as the end point in the industrial operation and, in most cases, the solid iron phase formed between 8 and 11 kg H_2/1000 kg intermediate slag. The mass fraction of Zn in the slag at end point is in the range of 0.1–0.9%, and mass fraction of Pb in the slag at end point is in the range of 0.000006–0.004% depending on the case. Distribution coefficients (liquid alloy/slag) for Ag at end point were between 8.5 and 11.4 for the 50, 25 and 10 vol.% H_2 cases, while the distribution coefficients for Au at end point were between 3.1×10^5 and 5.6×10^5 for the 50, 25 and 10 vol.% H_2 cases. This is in line with, if slightly less than, the measured distribution coefficients in the study by Avarmaa et al.[31] Looking at Fig. 1, which shows the reduction efficiency of hydrogen, we can see that the reduction efficiency near the end point of reduction is around 40%. This means that 60% of the hydrogen fed into the furnace passes the slag without participating in the reduction work. This is a consequence of the low stability of water as the reduction product of the process.

CONCLUSION

Every year millions of tons of non-ferrous residues are generated in primary production of metals. For a residue to be utilized, e.g., for construction purposes, it needs to be cleaned from hazardous substances and processed in a physically useful form. Also, the metal value can be valorized. In this study, the reduction of pretreated and desulfurized impure iron residue of industrial composition was studied using equilibrium calculations in FactSage

Figure 9 shows that the Ag that does not evaporate can mostly be found in the liquid alloy, while some also remained in the slag. Figure 10 shows

version 8.0 environment. Hydrogen was used as the reducing agent instead of carbon-based reducing agents. One of the big advantages of using H_2 as the reductant, instead of fossil fuels, is that the generated gases formed are composed of H_2O and H_2, which avoids the release of CO and CO_2.

The reduction process generated depleted slag, chemical flue dust and a liquid alloy phase, which tends to split into two immiscible compositions, depending on lead and sulfur concentrations of pre-treated iron residue. A higher total gas volume resulted in a decrease in the mass fraction of the liquid alloy phase when many minority components of the iron residue evaporated. An experimental study by Attah-Kyei et al. (2022) on pyrometallurgical processing of non-ferrous iron residue using hydrogen as the reducing agent shows the presence of a slag, gas, spinel and metal phase as well as an iron-rich phase, referred to as speiss, which formed after 10 min.[32]

In the beginning of the reduction, the slag included considerable amounts of Zn, Pb, As and Cu. As the reduction progressed, the slag got depleted of most of these elements. S, Bi, Pb, Ge and Zn evaporated fully from in flue dust in the off-gas train, while As, In, Sb and Ag evaporated partially. The remaining As deported strongly in the liquid alloy. The remaining In was mostly divided between the slag and liquid alloy. The Sb that did not evaporate could be found mostly in the liquid alloy and solid iron solution phase. The Ag that did not evaporate could be found mostly in the liquid alloy, while some also remained in the slag. Cu mostly deported in the liquid alloy as well as the solid iron solution phase, and almost none of it evaporated. The work shows clearly that valuable metals can be recovered. Achieving around 90% reduction of waste is significant and means the development of a new innovative process concept.

The reduction efficiency of hydrogen was calculated as a function of the degree of reduction, and it was around 100% in the beginning of the process. It was rapidly lowered close to 40% by the end point when solid iron was stabilized in the system. No significant difference in reduction efficiency of hydrogen was noted between the studied cases. A 40% reduction efficiency is low and far from ideal considering industrial applications at these temperatures. Further research on hydrogen is needed to address both the low reduction efficiency and the economic challenges of implementing hydrogen as reductant in a larger industrial scale at typical process temperatures of 1250–1350°C.

SUPPLEMENTARY INFORMATION

The online version contains supplementary material available at https://doi.org/10.1007/s11837-022-05653-x.

CONFLICT OF INTEREST

On behalf of all authors, the corresponding author states that there is no conflict of interest.

REFERENCES

1. ILZSG: International Zinc Study Group 2022 (accessed on July 15, 2022 at https://www.ilzsg.org/static/statistics.aspx).
2. M. Ruonala, K. Svens, J. Hammerschmidt, B. Saxén and E. Tuuppa, Latest Development in Zinc Processing. Paper presented at Lead-Zinc 2010, TMS, Vancouver, 2010, pp. 29–45.
3. K. Svens, *World Metall.–Erzmet.* 63, 136 (2010).
4. M.R.C. Ismael and J.M.R. Carvalho, *Miner. Eng.* 16, 31 https://doi.org/10.1016/S0892-6875(02)00310-2 (2003).
5. J.E. Dutrizac and S. Kaiman, *Can. Mineral.* 14, 151 (1976).
6. A. Pappu, M. Saxena, and S.R. Asolekar, *Sci. Total Environ.* 359, 232 https://doi.org/10.1016/j.scitotenv.2005.04.024 (2006).
7. S. Ju, Y. Zhang, Y. Zhang, P. Xue, and Y. Wang, *J. Hazard. Mater.* 192, 554 https://doi.org/10.1016/j.jhazmat.2011.05.049 (2011).
8. J. Salminen, J. Nyberg, M. Imris and B. M. Heegaard, Smelting Jarosite and Sulfur Residue in a Plasma Furnace. Paper presented at the 9th International Symposium on Lead and Zinc Processing, TMS, San Diego, 2020, pp. 391–403.
9. M. Rämä, S. Nurmi, A. Jokilaakso, L. Klemettinen, P. Taskinen, and J. Salminen, *Metals* 8, 744 https://doi.org/10.3390/met8100744 (2018).
10. S. Wegscheider, S. Steinlechner, and M. Leuchtenmüller, *JOM* 69, 388 https://doi.org/10.1007/s11837-016-2192-7 (2017).

11. S. Creedy, A. Glinin, R. Matusewicz, S. Hughes, and M. Reuter, *World Metall. Erzmet.* 66, 230 (2013).
12. L. Hoeber and S. Steinlechner, *Clean. Engin. Technol.* 4, 100214 https://doi.org/10.1016/j.clet.2021.100214 (2021).
13. P. Asokan, M. Saxena, and S.R. Asolekar, *J. Hazard. Mater.* 137, 1589 https://doi.org/10.1016/j.jhazmat.2006.04.054 (2006).
14. A. Cheilas, M. Katsioti, A. Georgiades, O. Malliou, C. Teas, and E. Haniotakis, *Cem. Concr. Compos.* 29, 263 https://doi.org/10.1016/j.cemconcomp.2006.12.005 (2007).
15. A. Pappu, M. Saxena, and S.R. Asolekar, *Build. Sci.* 42, 2311 https://doi.org/10.1016/j.buildenv.2006.04.015 (2007).
16. D. Calla-Choque, F. Nava-Alonso, and J.C. Fuentes-Aceituno, *J. Hazard. Mater.* 317, 440 https://doi.org/10.1016/j.jhazmat.2016.05.085 (2016).
17. P. Kangas, M. Nyström, I. Orko, P. Koukkari, P. Saikkonen and J. Rastas, The Jarogain Process for Metals Recovery from Jarosite and Electric Arc Furnace Dust, (VTT Technical Research Centre of Finland, Espoo, 2017) https://publications.vtt.fi/pdf/technology/2017/T317.pdf.
18. J.M.N. van Kasteren and J.P. Lotens, *Resour. Conserv. Recycl.* 14, 35 https://doi.org/10.1016/0921-3449(94)00053-8 (1995).
19. B.-S. Kim, S.-B. Jeong, J.-C. Lee, D. Shin, and N.-I. Moon, *Mater. Trans.* 53, 985 https://doi.org/10.2320/matertrans.M2012006 (2012).
20. J. Wood, J. Conveney, J. Helin, G. Xu and S. Xicheng, The Outotec Direct Zinc Smelting Process. Paper presented at European Metallurgical Conference, GDMB, Clausthal-Zellerfeld, 2015.
21. K. Verscheure, M. van Camp, B. Blanpain, P. Wollants, P. Hayes, and E. Jak, *Metall. Mater. Trans. B* 38B, 21 https://doi.org/10.1007/s11663-006-9010-5 (2007).
22. H. Spratt, L. Rintoul, M. Avdeev, and M. Wayde, *J. Thermal Anal. Calorim.* 115, 101 https://doi.org/10.1007/s10973-013-3213-1 (2014).
23. I.-H. Jung and M.-A. Van Ende, *Metall. Mater. Trans. B* 51, 1851 https://doi.org/10.1007/s11663-020-01908-7 (2020).
24. U.R. Kattner, *JOM* 49(12), 14 (1997).
25. D. Lindberg, R. Backman, P. Chartrand, and M. Hupa, *Fuel Process. Technol.* 105, 129 https://doi.org/10.1016/j.fuproc.2011.08.008 (2013).
26. J. Lehmann, I.-H. Jung and L. Zhang, (2012). The main thermo-statistical models of metallurgical slgas: theory and applications. Proc. Molten Slags and Fluxes 2012. Retrieved from https://www.pyrometallurgy.co.za/MoltenSlags2012/W158.pdf.
27. A.D. Pelton, G. Eriksson, and C.W. Bale, *Calphad* 33, 679 https://doi.org/10.1016/j.calphad.2009.08.005 (2009).
28. C.W. Bale, E. Bélisle, P. Chartrand, S.A. Decterov, G. Eriksson, K. Hack, I.-H. Jung, Y.-B. Kang, J. Melançon, A.D. Pelton, C. Robelin, and S. Petersen, *Calphad* 23, 295 https://doi.org/10.1016/j.calphad.2008.09.009 (2009).
29. D. Sukhomlinov, L. Klemettinen, O. Virtanen, Y. Lahaye, P. Latostenmaa, A. Jokilaakso, and P. Taskinen, *Can. Metall. Q.* 59, 67 https://doi.org/10.1080/00084433.2019.1710386 (2020).
30. D.R. Swinbourne and T.S. Kho, *Metall. Mater. Trans. B* 43, 823 https://doi.org/10.1007/s11663-012-9652-4 (2012).
31. K. Avarmaa, H. O'Brien, L. Klemettinen, and P. Taskinen, *J. Mater. Cycles Waste Manag.* 22, 642. https://doi.org/10.1007/s10163-019-00955-w (2020).
32. D. Attah-Kyei, L. Klemettinen, R. Michallik, J. Salminen, P. Taskinen, and D. Lindberg, *Metall. Mater. Trans. B*, 53, 3775. https://doi.org/10.1007/s11663-022-02640-0 (2022).